SYNTHESIS, CHARACTERIZATION AND MAGNETIC PROPERTIES OF LA$_{0.7}$SR$_{0.3}$MNO$_3$(LSMO) NANOPARTICLES BY CITRATE PRECURSOR TECHNIQUE.

Rohit kumar[1], Prof.Arun Kumar Singh[2], Dr. Deepak Kumar [3] ,Amit kumar Bharti,[4] Krishnandan Ray, [5]prof. surendra Kumar[6]

1,,4,5ResearchScholar,UniversityDepartmentofPhysics,L.N.MithilaUniversity,Darbhanga.

2,6 Prof.,UniversityDepartmentofPhysics,L.N.MithilaUniversity,Darbhanga

3.AssistantProfessor,UniversityDepartmentofPhysics,L.N.MithilaUniversity, Darbhanga

Email:-deep9435@gmail.com, rkroy190@gmail.com, singharun63@gmail.com

Abstract:-The structural and magnetic characteristics of La$_{0.7}$Sr$_{0.3}$MnO$_3$(LSMO), which is produced using sol-gel, solution combustion, and The material's morphology and structure, which define its overall properties, are controlled by the synthesis process; The synthesis begins with metal nitrates as the metal source, citric acid as the chelating agent, propylene glycol as the solvent, and distilled water (DW) as the precursor. With the use of SQUID magnetometry, X-ray photoelectron microscopy (XPS), X-ray diffraction (XRD), and crystallinity, the formation mechanism, crystal structure, Phase composition, and magnetic characteristics are examined. A crystallite size of around 17.9 nm has been confirmed by XRD measurements to be the phase of pure nanocrystalline La$_{0.7}$Sr$_{0.3}$MnO$_3$The 300K and 5K magnetic characteristics are studied. La$_{0.7}$Sr$_{0.3}$MnO$_3$(LSMO) nanoparticles exhibit superparamagnetic behavior; coercivity and remanence are negligible. The M-H curvesdemonstrate that the samples' nanoparticles have ferromagnetic order, and the Arrott plots suggest that ferromagnetic order increases with increasing particle size.

Keywords: Manganite, Magnetic nanoparticles**.** Sol-gel-synthesis, nanoparticles. Super paramagnetism, superspin glass.

Introduction:-The properties of materials at the nanoscale differ significantly from those at the bulk scale, which makes them useful for use in electromagnetic shielding, optoelectronic devices, magnetic data storage, sensors, and other applications. [1-8] The origins of mixed-valence manganites may be traced back to the 1950s, when G. H. Jonker and J. H. Van Santen created these materials as polycrystals in order to study manganites' magnetic characteristics [9]. They discovered that the perovskite structure of these materials has FM characteristics. The cubic perovskite structure is seen in Figure 1. Re1-xTxMnO3, where T is a divalent alkaline earth element and Re is a trivalent rare earth element, is the usual formula for manganese oxide [10]. Large blue and little blue represent the A and B sites, respectively.At the centre of each of the cube's faces are green spheres and oxygen, respectively. Using 12-fold oxygen coordination, the Re and T elements are situated at the A sites. When a cube is in the octahedral oxygen coordination, cations of Mn are located at its B sites. To retain charge neutrality, some Mn^{3+} in the perovskite structure is converted to Mn^{4+} by the divalent Re element, which takes the place of the T element. x and 1-x, respectively, are the stiochiometric portions of Mn^{3+} and Mn^{4+}·It has been claimed that the lattice mismatch

between LSMO's cubic structure to transform into a pseudo-cubic structure, changing the lattice parameter of the sample. The lattice parameters of the pseudo-cubic structure area = b = 3.905 Å and c = 3.846 Å with α = β = 90° and γ = 90.87° [11,12].
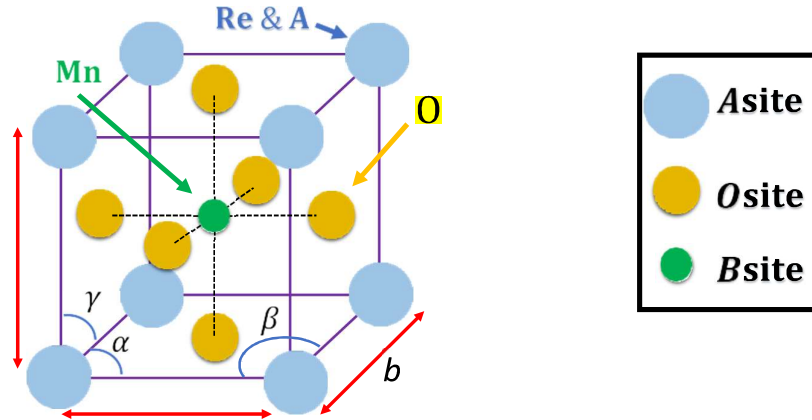

Figure 1: Structure of a Cubic Perovskite.

The Mn atom is half-filled in its 3d orbital and has the electrical configuration$1s^2 2s^2 2p^6 3s^2 3p^6 3d^5 4s$. The 3-fold orbital degeneracy of the t2g and eg degenerate states is broken into three t2g and two eg states because of the oxygen atoms' crystal field. The t2g states have lower energies concerning the eg states because they experience less coulomb repulsion than the eg states, which are located between the points of the cartesian coordinate system between the ligands. This is because the eg states point directly at the ligands. Hund's first rule, which specifies that the maximal value of spin (S) must be satisfied, states that the electrons fill the orbital states of Mn^{3+} and Mn^{4+}. For Mn^{3+} and Mn^{4+}, this means that their S values are 2 and 3/2, respectively. The T2gThe electron density of the Mn^{4+} level is three, while that of the eG is zero. Manganites' magnetic and electricalcharacteristics are determined by the electron configuration of Mn cations contained in octahedral oxygen coordination [10]. The particle size distribution, finite-size effect, dipolar or exchange interaction between the particles, and particle shape all have a significant impact on the magnetic characteristics of nanoparticles [13]. Since densely packed nanoparticles are used in many magnetic nanoparticles applications, it is crucial to understand how interactions between nanoparticles affect the physical characteristics of these systems [2, 14]. Every particle has a big magnetic moment, or "super spin," if the particle size is less than the size of a single domain [2, 8, 15]. The effect of superparamagnetic behaviour is that,The electron density of the Mn4+ level is three, while that of the eG is zero. The Mn cation electron configuration is embedded in noninteracting super spins of octahedral oxygen. [16–8]. In the superparamagnetic state, the magnetic nanoparticles undergo a superparamagnetic relaxation process in which their magnetization direction rapidly fluctuates rather than fixed along a certain direction. This is because, while the magnetic order remains within the particles, each particle behaves like a paramagnetic atom. The blocking temperature is the point at which a nanoparticle's magnetic anisotropy energy is overcome by thermal activation [8, 13]. The system of interacting super spins exhibits the super spin glass when the fully frustrated and random interactions between the super spins get strong enough.actions in very cold temperatures [2, 8, 13, 15, 17]Ac

magnetic susceptibility is used to investigate the magnetic properties of magnetic nanoparticles in terms of their kinetics. Superparamagnetic and superspin materials can be distinguished using this technique. In this study, we synthesised LSMO by chemical methods (sol–gel, solution combustion). These methods provide nanocrystalline LSMO, and the impact of the synthesis process on the structural and magnetic characteristics of LSMO has been thoroughly investigated.

2 Experimental techniques and synthesized samples:-

The sol-gel process [18] was used to create $La_{0.7}Sr_{0.3}MnO_3$(LSMO) nanoparticles. Ten-fold lanthanum nitrate ($La(NO_3)_3.6H_2O$), tetrahydrate manganese nitrate ($Mn(NO_3)2.4H2_O$), and strontium nitrate ($Sr(NO_3)$)(all from Sigma-Aldrich, USA),There were two analytical-grade propylene glycol (Thomas Baker, India) and citric acid (Merck, Germany). Each metal nitrate's stiochiometric quantity was first dissolved in a different batch of deionized water to form the precursor solution. Propylene glycol and citric acid were also added in a 1:1 mole ratio to the preparatory solution containing the metal nitrates. All of the liquid evaporated and black precursor powder was created by heating the mixture to 90 °C on a thermal plate while stirring it magnetically. For the purpose of obtaining well-crystallized LSMO nanoparticles, the precursor powder was heated to 800 °C for three hours while in an ambient atmospherepace of two degrees Celsius each minute. Using an XRD pattern with a CuKα radiation source in the 2θ scan range of 10° to 90°, the phase formation and crystal structure of the powders were examined.
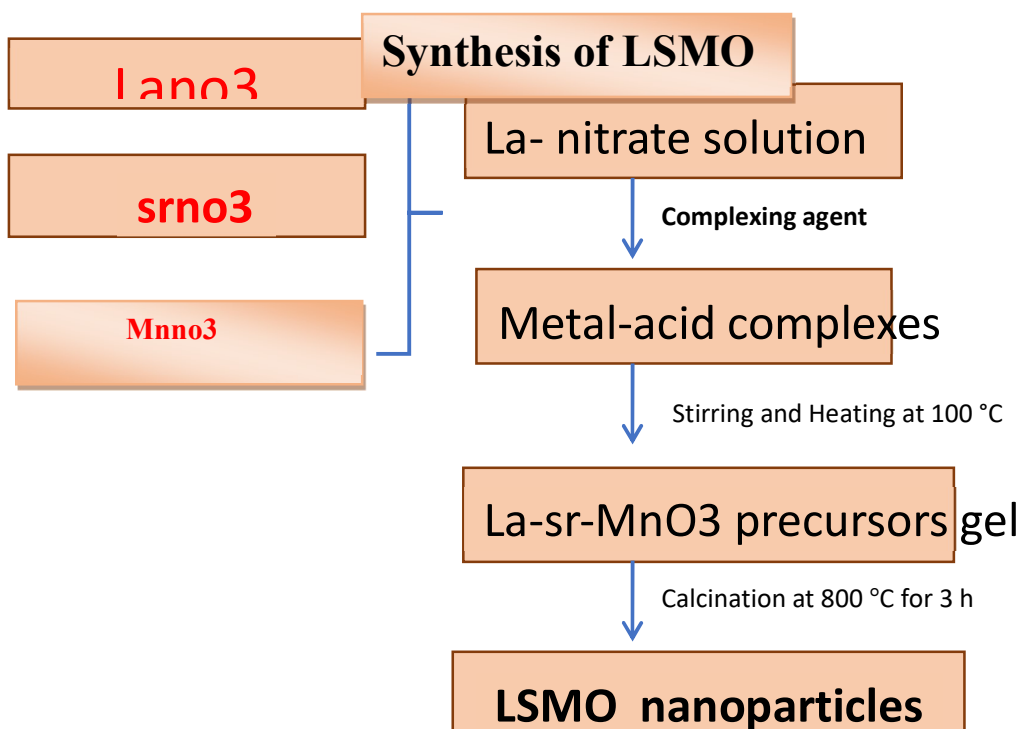

Fig.2 Flow chart of the preparation of $La_{0.7}Sr_{0.3}MnO_3$(LSMO) nanoparticles by Solution combustion technique

3Results and discussions:-
3.1. Structural analysis:-

The sample's XRD pattern is displayed in Figure 2. The FULLPROF programme was used to carry out Rietveld refinement in order to examine the x-ray data [18]. After refining, the unit cell's lattice parameters were determined to be a = 5.4736 Å and c = 13.3097 Å, with a goodness of fit χ2 of 1.25. The sample is of a single phase, as confirmed by the refinement results (inset of Figure 1) conforming to the rhombohedral structure specifiedby the R-3C space group [19]. Using the Debye Scherrer formula, the values of crystallite size (D) were determined from the half-width (FWHM-Full Width Half Maximum) of the most intense peak.

$$d = \frac{K\lambda}{\beta cos\theta}$$

where λ is 1.541 8 Å, B(2θ) is FWHM, and k is a constant (0.94)[20, 21].The approximate values ofFor the sample sintered at 800 °C for three hours, the crystallite size was found to be 20 nm. The pellets (made of nanoparticles) used in this investigation were sintered at 800 °C for three hours. XRD data for LaFeO3(LSMO) nps refined using Rietveld technique. The computed pattern (Ical) is displayed in solid lines, the experimental data (Iobs) are represented by circles, and the difference between the two patterns (Iobs – I cal) is represented by the bottom curve. The vertical barrepresentthePbnm space group's Bragg reflection.
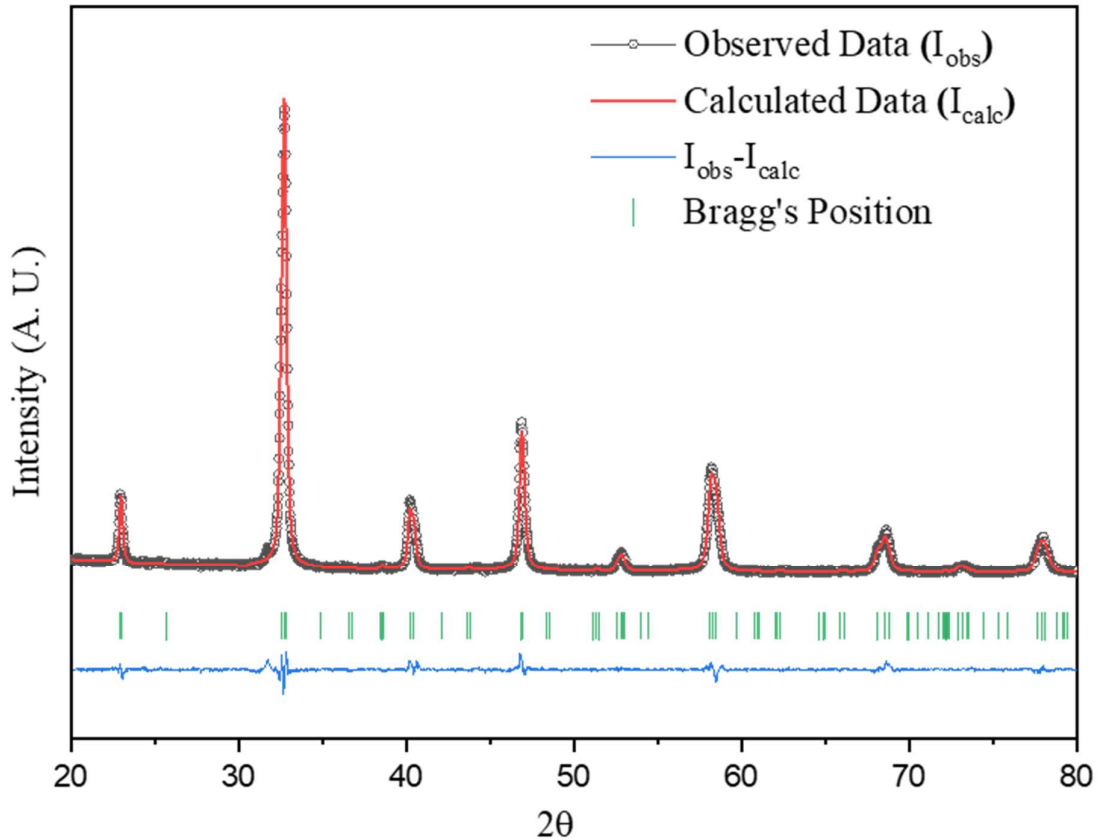

Fig 3. (a) XRD data for LaFeO3(LSMO) nps refined using Rietveld method. The computed pattern (Ical) is displayed in solid lines, the experimental data (Iobs) are represented by circles,

and the difference between the two patterns (Iobs – I cal) is represented by the bottom curve. The vertical bars represent the Pbnm space group's Bragg reflection.
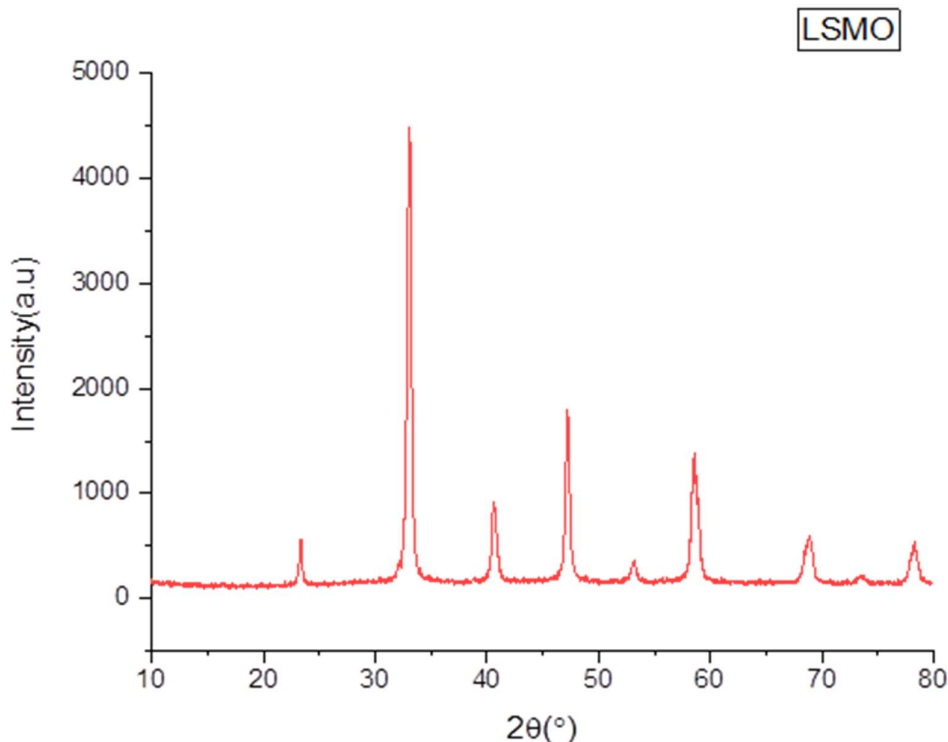
Fig.3 (b) XRD Pattern of LSMO at room temperature.

Table 1: Structural Parameters of La$_{0.7}$Sr$_{0.3}$MnO$_3$(LSMO) Derived from the Rietveld refinement of XRD Pattern

| Parameters	Sample(LSMO)
a (Å)	5.4736
b (Å)	5.4736
c (Å)	13.3097
Volume (Å)3	346.022
Space group	(Rhombohedral) R-3C
Crystallite size (nm)	17.9

The surface area (An) to volume (Vn) ratio of the nanocrystal, or A$_n$/V$_n$, is known to increase with decreasing particle size in roughly spherical particles with sizes in the nanometer range. In the case of doped manganites, it has generally been found that when the particle size reduces from bulk (roughly greater than 150 nm) to nano sizes (roughly less than 50 nm), there is a corresponding decrease in crystallite size and contraction in unit cell volume. This phenomenon is caused by a decrease in the sintering time and/or temperature of the ceramic pellets.The shift

of XRD peaks indicates that the lattice spacing of the hexagonal unit cell decreases as a result of the decrease in lattice parameters.

the larger value of 2θ while applying a shorter sintering time and lower temperature for the ceramic pellets. The internal pressure, or Pi, characteristics can be used to explain the change in peak position to the higher angle that occurs with decreasing crystallite size. As the size of the crystallites decreases, the internal pressure, ΔPi = ∘An/Vn, changes. The formula for the link between the ratio An/Vn and average crystallite size (ádñ) is An/Vn∧□ádñ-1 [05].As a consequence, when the size of the crystallite decreases, the ratio An/Vn rises and the system's internal pressure increases. This causes the unit cell volume to contract in every direction. As a result, the nano-size sample's total lattice properties decrease. The reciprocal diffraction lines in the XRD patternThus, the XRD pattern shows a signature of a reduction in the unit cell's lattice parameter together with small shifts in peak positions towards the higher value of 2θ.The observed trend in our investigation, utilising varying sintering conditions, aligns with the previously documented XRD pattern for distinct doped manganite systems [06, 07].

3.2 XPS analysis

The chemical makeup of the sol-gel, combustion-produced LSMO samples was examined using X-ray photoelectron spectroscopy (XPS). Fig. 3 displays the O (oxygen)1s spectra. There are two distinct peaks in the O 1s spectra that are associated with the different the surface. kinds of oxygen. O II (531–532.8 eV) is the high energy peak, attributed to the surface adsorbed oxygen or hydroxyl group, while O I (529–530.7 eV) is the lower binding energy peak. The area under the peak O II / O I ratio can be used to estimate the number of oxygen vacancies in the sample [32]. O II/O I ratio, which was derived from the LSMO, the deconvolution of the XPS spectra is 1.01, 1.12, and 0.88. So, the chemical makeup of the was examined using X-ray photoelectron spectroscopy (XPS). According to the XPS research, the amount of oxygen vacancies in the LSMO will be.
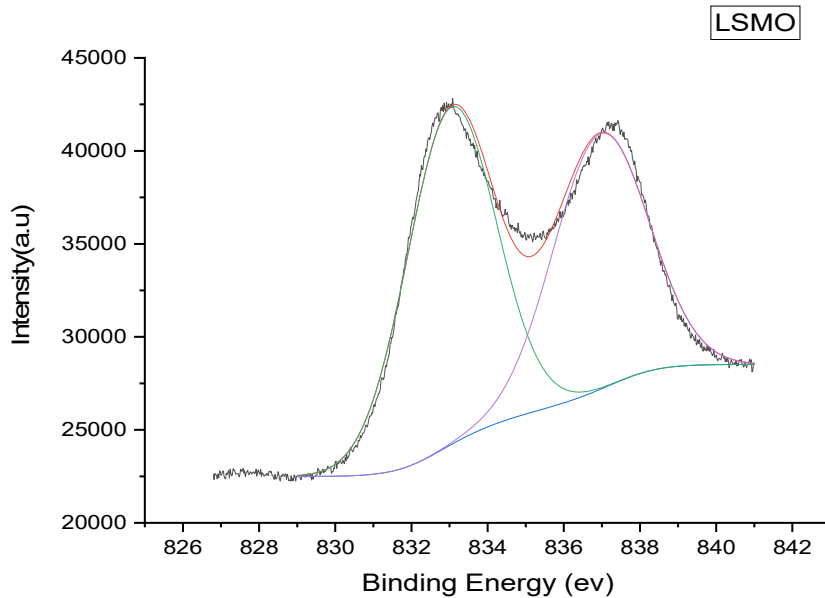
Fig. 4 shows that a comparison between intensity (a.u) and Binding energy of LSMO

3.3 Magnetic characteristics:-Zener's double exchange model [11] explains the magnetic behaviour of the manganites. Manganese cations' d-orbitals indirectly couple to one another, which forms the basis of the suggested mechanism. In this mechanism, as opposed to the super-exchange mechanism, where the two nearest magnetic ionic neighbours are Mn cations with the same valence, the two Mn cations, Mn3+ and Mn4+, are separated by an oxygen atom [12,13]. For Mn cations in the double-exchange, there are two conceivable degenerate states. Here are the states: [14] T2: Mn4+O2−Mn3+, and T1: Mn3+O2−Mn4+. In T1, an electron moves from the O2- 2p orbital to the vacant eg orbital of Mn4+, and concurrently, an electron moves from Mn3+ to the O2- 2p orbital, lowering

based on this orbital's energy, and $T1$ transforms into $T2$. Between these two degenerate states, the magnetic system is resonant. In Figure 1.5, an electron hopping diagram from O2-to Mn4+ and Mn3+ to O2-is presented. All of the magnetic moments on both Mn cations must be parallel, and the hopped electron must have the same spin as the other electrons, according to Hund's rule. This results in the lowest energy levels and a ground state of FM.
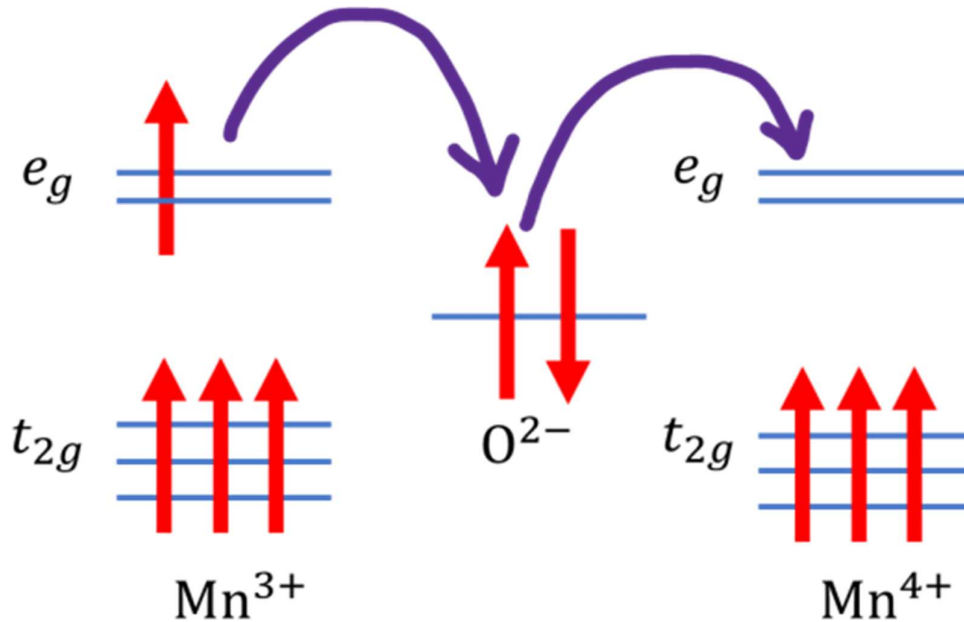
The Mn cations double-exchange is shown in Figure 5(a) [8,14].

It is generally known that Re1-xAxMnO3 compounds include a double-exchange process. We can achieve various magnetic phases and electrical characteristics by varying the composition of these compounds. The TC of these materials is dependent on the average ionic radius of the cation in the A position and the doping level x, as demonstrated by Santen and Jonker [7,15]. It was demonstrated that La1-xSrxMnO3 has the greatest possible TC and Ms value, with an ideal ratio of x ~ 0.3. For spintronics [16], multiferroic tunnel junctions [17], colossal magnetoresistance [18], resistive switching memory devices [19], ferroelectric/ferromagnetic systems [20], and heterostructures [21], La0.7Sr0.3MnO3 (LSMO) films are promising possibilities. The greatest magnetic efficiency cannot always be achieved, despite the wide range of applications for LSMOs.

To study the magnetic behavior of the samples, the field dependence of magnetization has been measured at room temperature (295 K). The field dependence of the magnetization for samples are shown in Fig. 4. From Fig. 4, the M–H curve of sample shows superparamagnetic behavior, without noticeable remanence and coercivity. However, the M–H curve of samples show that the magnetization has a ferromagnetic typebehavior with a small hysteresis loop and a low coercive field. It can be seen from Fig. 4 that the magnetization is not saturated in the applied magnetic fields up to 8.5 kOe which is due to the noncollinear surface spins of nanoparticles. The existence of the coercive field in the magnetization of samples indicates some part of the particles are blocked due to the overcoming of the thermal energy by their anisotropy energy at room temperature. Thisis due to the size distribution of magnetic nanoparticles, and consequently these samples have different blocking/freezing temperatures. We have also applied the well-known Arrott plot (M^2 versus H/M) for samples as shown in the lower insets of Fig. 4. From Fig. 4, Arrott plot shows a strong convex curvature

with a finite spontaneous magnetization which is a signature of ferromagnetic phase of the samples [26, 27]. Spontaneous magnetization can be estimated by linear fitting of the high magnetic field part of the M^2–H/M curve and intercepts it with the M^2 axis. By increasing the particle size, the spontaneous magnetization and curvature are increased which indicates that the magnetic order in the samples
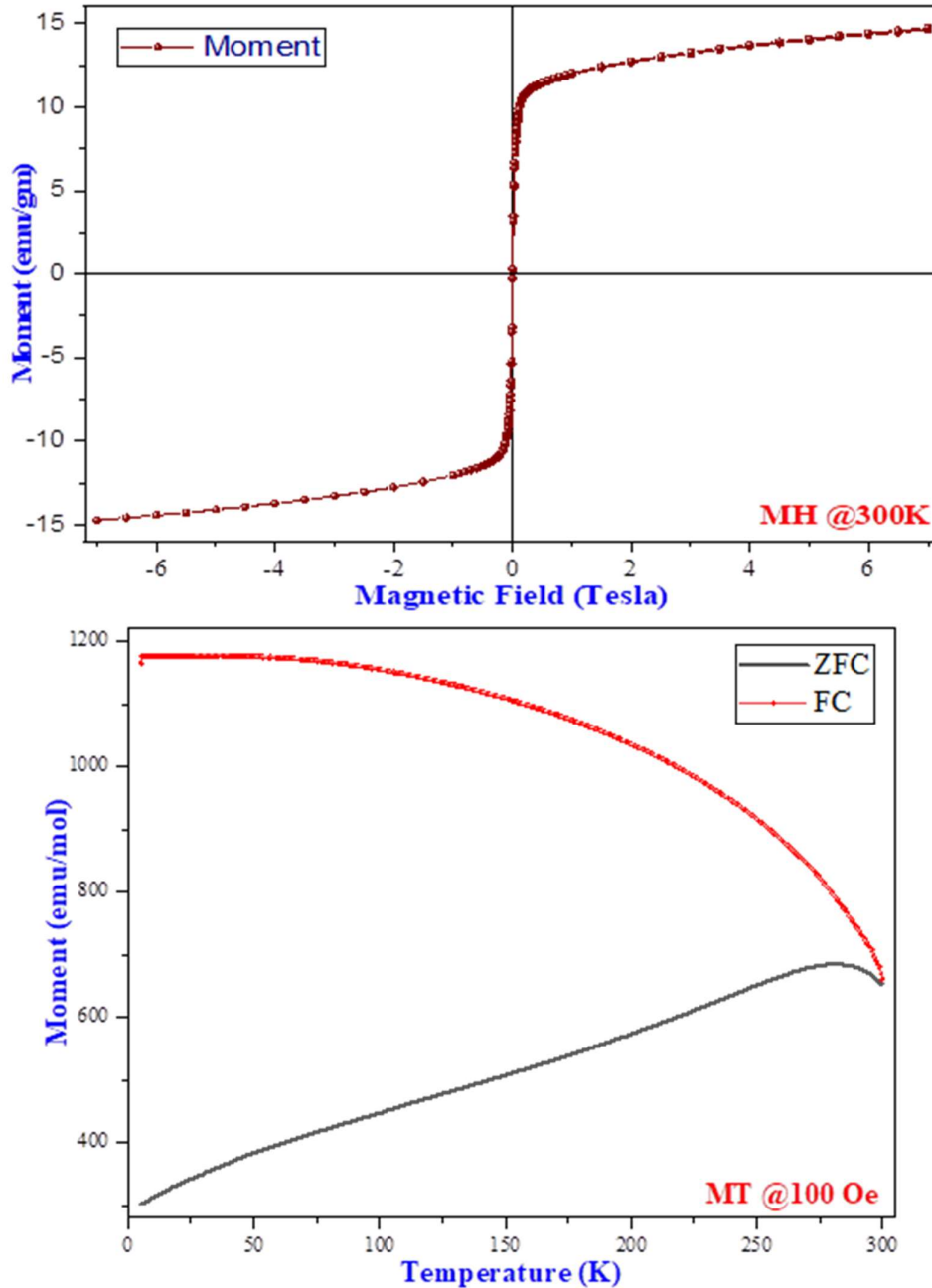
Fig.5(b) M-H loop of LSMO

Fig.5(c) M-T(ZFC-FC)measurement of the LSMO

4.Conclusions:-

To determine the magnetic behaviour of LSMO nanoparticles, summarise the acquired data. The samples' nanoparticles have ferromagnetic order, as demonstrated by the M-H curves, and the Arrott plots demonstrate that ferromagnetic order increases with increasing particle size.

Superparamagnetic and spin glass systems exhibit these behaviours. Neel-Brown, Vogel-Fulcher, and critical slowing down are three phenomenological models and empirical criteria parameters that are used to characterise the magnetic dynamic behaviour of magnetic nanoparticle systems based on the strength of the interparticle interaction. For superparamagnetic systems, the Néel-Brown and Vogel-Fulcher laws are applied. For both spin and superspin glasses, the Vogel-Fulcher law is applied. Utilising the Neel-Brown model to fit the experimental data results in unphysical lowvalues for the relaxation time ($\tau_0 \approx 10^{-54}$–10^{-128} s) of the samples and suggests that the LSMO nanoparticles interact strongly with one another. Strong interactions between LSMO nanoparticles are confirmed by the excellent agreement between the experimental data and the Vogel-Fulcher model. The relaxation time and magnetic anisotropy constant for our samples with varying particle sizes have been determined by fitting the experimental data with this model. The results that were achieved match the results that were published. Strong nanoparticle contact is also evident from the values of that were obtained. Our samples may exhibit superspin glass behaviour, as the essential slowing down hypothesis fits the experimental data quite well. Even yet, it is challenging to separate true spin glass systems from interacting superparamagnetic systems.

5..Recognizations

Reference:

1. N. Thorat, K. Shinde, S. Pawar, K. Barick, C. Betty, R. Ningthoujam, Polyvinyl alcohol: an efficient fuel for the synthesis of superparamagnetic LSMO nanoparticles for biomedical application. Dalton Trans. **41**(10), 3060–3071 (2012)

2. H. Liang, J. Liu, Y. Zhang, L. Luo, H. Wu, Ultra-thin broccoli- like SCFs@TiO2 one-dimensional electromagnetic wave absorbing material. Compos. B Eng. **178**, 107507 (2019)

3. H. Wu, D. Lan, B. Li, L. Zhang, Y. Fu, Y. Zhang, H. Xing, High-entropy alloy@ air@ Ni–NiO core-shell microspheres for electromagnetic absorption applications. Compos. B Eng. **179**, 107524 (2019)

4. D. Lan, M. Qin, J. Liu, G. Wu, Y. Zhang, H. Wu, Novel binary cobalt nickel oxide hollowed-out spheres for electromagnetic absorption applications. Chem. Eng. J. **382**, 122797 (2020)

5. J. Liu, H. Liang, Y. Zhang, G. Wu, H. Wu, Facile synthesis of ellipsoid-like MgCo2O4/ Co3O4 composites for strong wideband microwave absorption application. Compos. B Eng. **176**,107240 (2019)

6. K. Omri, J. El Ghoul, O. Lemine, M. Bououdina, B. Zhang, L.El Mir, Magnetic and optical properties of manganese doped ZnO nanoparticles synthesized by sol–gel technique. Superlattice Microstruct. **60**, 139–147 (2013)

7. K. Omri, O. Lemine, L. El Mir, Mn doped zinc silicate nanophosphor with bifunctionality of green–yellow emission and magnetic properties. Ceram. Int. **43**(8), 6585–6591 (2017)

8. K. Omri, N. Alonizan, Effects of ZnO/Mn concentration on the micro-structure and optical (Navin and Kurchania 2021)properties of ZnO/Mn–TiO2 nanocomposite for applications in photo-catalysis. J. Inorg. Organomet. Polym Mater. **29**(1), 203–212 (2019)

[9] G.H. Jonker, J.H. Van Santen, Ferromagnetic compounds of manganese with perovskite structure, Physica. 16 (1950) 337–349. https://doi.org/https://doi.org/10.1016/0031-8914(50)90033-4.

[10] N. Izyumskaya, Y. Alivov, H. Morkoç, Oxides, oxides, and more oxides: High-oxides, ferroelectrics, ferromagnetics, and multiferroics, Crit. Rev. Solid State Mater. Sci. 34 (2009) 89–179. https://doi.org/10.1080/10408430903368401.

[11] H. Boschker, M. Huijben, A. Vailionis, J. Verbeeck, S. van Aert, M. Luysberg, S. Bals, G. van Tendeloo, E.P. Houwman, G. Koster, D.H.A. Blank, G. Rijnders, Optimized fabrication of high-quality La 0.67 Sr 0.33 MnO 3 thin films considering all essential characteristics, J. Phys. D. Appl. Phys. 44 (2011) 205001. https://doi.org/10.1088/0022-3727/44/20/205001.

[12] A. Vailionis, H. Boschker, W. Siemons, E.P. Houwman, D.H.A. Blank, G. Rijnders, G. Koster, Misfit strain accommodation in epitaxial ABO3 perovskites: Lattice rotations and lattice modulations, Phys. Rev. B Condens. Matter Mater. Phys. 83 (2011). https://doi.org/10.1103/PhysRevB.83.064101

[13]. M. Soleymani, M. Edrissi, A.M. Alizadeh, Thermosensitive polymer-coated La0.73Sr0.27MnO3 nanoparticles: potential applications in cancer hyperthermia therapy and magnetically activated drug delivery systems. Polym. J. **47**(12), 797 (2015)

[14]. K. Shinde, S. Pawar, N. Deshpande, J. Kim, Y. Lee, S. Pawar, Magnetocaloric effect in LSMO synthesized by combustionroute. Mater. Chem. Phys. **129**(1–2), 180–182 (2011)

[15]. H.A. Reshi, A.P. Singh, S. Pillai, R.S. Yadav, S. Dhawan, V. Shelke, Nanostructured La0.7Sr0.3MnO3 compounds for effective electromagnetic interference shielding in the X-band frequency range. J. Mater. Chem. C **3**(4), 820–827 (2015)

[16]. K. Miyazaki, N. Sugimura, K. Matsuoka, Y. Iriyama, T. Abe, M. Matsuoka, Z. Ogumi, Perovskite-type oxides La1−xSrxMnO3 for cathode catalysts in direct ethylene glycol alkaline fuel cells. J. Power Sources **178**(2), 683–686 (2008)

[17]. A. Molinari, P.M. Leufke, C. Reitz, S. Dasgupta, R. Witte, R. Kruk, H. Hahn, Hybrid supercapacitors for reversible control of magnetism. Nat. Commun. **8**, 15339 (2017)

[18] Srivastav S Kand GajbhiyeNS 2012 J. Am. Ceram. Soc. 95 3678

[19] Rodríguez-Carvajal J 1993 Physica B: Condensed Matter 192 55

[20] Radaelli P, Iannone G, Marezio M, Hwang H, Cheong S, Jorgensen J and ArgyriouD1997 Phys. Rev. B 56 8265

[21] Warren B E 1969 X-ray Diffraction (New York: Dover)

[22] Cha J and ParkK2017 Ceram. Int. 43 16159

[23] ShankarKS, Kar S, SubbannaGandRaychaudhuriA 2004 Solid State Commun. 129 479

[24] Dey P and Nath T 2006 Phys. Rev. B 73 214425

[25] VenkataiahGand Reddy PV2009 Phase Transit. 82 156

[26] C. Zener, Interaction Between the *d* Shells in the Transition Metals, Phys. Rev. 81 (1951) 440–444. https://doi.org/10.1103/PhysRev.81.440

[27] J.B. Goodenough, Theory of the Role of Covalence in the Perovskite-Type Manganites [La, M(II)]MnO3, Phys. Rev. 100 (1955) 564–573. https://doi.org/10.1103/PhysRev.100.564.

[28] P.W. Anderson, Antiferromagnetism. Theory of Superexchange Interaction, Phys. Rev. 79 (1950) 350–356. https://doi.org/10.1103/PhysRev.79.350.

[29] C. Zener, Interaction between the d-Shells in the Transition Metals. II. Ferromagnetic Compounds of Manganese with Perovskite Structure, Phys. Rev. 82 (1951) 403–405. https://doi.org/10.1103/PhysRev.82.403.

[30] J.H. Van Santen, G.H. Jonker, Electrical conductivity of ferromagnetic compounds of manganese with perovskite structure, Physica. 16 (1950) 599–600. https://doi.org/https://doi.org/10.1016/0031-8914(50)90104-2.

[31] J. Huang, H. Wang, X. Sun, X. Zhang, H. Wang, Multifunctional La0.67Sr0.33MnO3 (LSMO) Thin Films Integrated on Mica Substrates toward Flexible Spintronics and Electronics, ACS Appl. Mater. Interfaces. 10 (2018) 42698–42705. https://doi.org/10.1021/acsami.8b16626.

[32] V. Borisov, S. Ostanin, I. Mertig, Multiferroic properties of the PbTiO3/La2/3Sr1/3MnO3 interface studied from first principles, J. Phys. Condens. Matter. 29 (2017) 175801. https://doi.org/10.1088/1361-648X/aa6318.

[33] Y.H. Ren, M. Ebrahim, H.B. Zhao, G. Lüpke, Z.A. Xu, V. Adyam, Q. Li, Time-resolved optical studies of spin and quasiparticle dynamics in colossal magnetoresistance materials: La0.67Ca0.33MnO3 and Sr2FeMoO6, Phys. Rev. B. 78 (2008) 14408. https://doi.org/10.1103/PhysRevB.78.014408.

[34] C. Moreno, C. Munuera, S. Valencia, F. Kronast, X. Obradors, C. Ocal, Reversible resistive switching and multilevel recording in La0. 7Sr0. 3MnO3 thin films for low cost nonvolatile memories, Nano Lett. 10 (2010) 3828–3835.